AGU PUBLICATIONS

JGR

Journal of Geophysical Research: Oceans

RESEARCH ARTICLE

10.1002/2015JC011037

Special Section:
Physical Processes Responsible for Material Transport in the Gulf of Mexico for Oil Spill Applications

Tracking the *Hercules 265* marine gas well blowout in the Gulf of Mexico

Isabel C. Romero[1], Tamay Özgökmen[2], Susan Snyder[1], Patrick Schwing[1], Bryan J. O'Malley[1], Francisco J. Beron-Vera[2], Maria J. Olascoaga[2], Ping Zhu[3], Edward Ryan[2], Shuyi S. Chen[2], Dana L. Wetzel[4], David Hollander[1], and Steven A. Murawski[1]

[1]College of Marine Science, University of South Florida, St. Petersburg, Florida, USA, [2]Rosenstiel School of Marine and Atmospheric Science, University of Miami, Miami, Florida, USA, [3]Department of Earth and Environment, Florida International University, Miami, Florida, USA, [4]Mote Marine Laboratory, Sarasota, Florida, USA

Abstract On 23 July 2013, a marine gas rig (*Hercules 265*) ignited in the northern Gulf of Mexico. The rig burned out of control for 2 days before being extinguished. We conducted a rapid-response sampling campaign near *Hercules 265* after the fire to ascertain if sediments and fishes were polluted above earlier baseline levels. A surface drifter study confirmed that surface ocean water flowed to the southeast of the *Hercules* site, while the atmospheric plume generated by the blowout was in eastward direction. Sediment cores were collected to the SE of the rig at a distance of ~0.2, 8, and 18 km using a multicorer, and demersal fishes were collected from ~0.2 to 8 km SE of the rig using a longline (508 hooks). Recently deposited sediments document that only high molecular weight (HMW) polycyclic aromatic hydrocarbon (PAH) concentrations decreased with increasing distance from the rig suggesting higher pyrogenic inputs associated with the blowout. A similar trend was observed in the foraminifera *Haynesina germanica*, an indicator species of pollution. In red snapper bile, only HMW PAH metabolites increased in 2013 nearly double those from 2012. Both surface sediments and fish bile analyses suggest that, in the aftermath of the blowout, increased concentration of pyrogenically derived hydrocarbons was transported and deposited in the environment. This study further emphasizes the need for an ocean observing system and coordinated rapid-response efforts from an array of scientific disciplines to effectively assess environmental impacts resulting from accidental releases of oil contaminants.

Key Points:
- Atmospheric and surface water circulations were modeled
- Combustion byproducts were found in sediments and fishes after *Hercules 265* rig blowout
- Baseline contamination levels are imperative for environmental impact studies

Supporting Information:
- Supporting Information S1

Correspondence to:
I. C. Romero,
isabelromero@mail.usf.edu

Citation:
Romero, I. C., et al. (2016), Tracking the *Hercules 265* marine gas well blowout in the Gulf of Mexico, *J. Geophys. Res. Oceans*, *121*, 706–724, doi:10.1002/2015JC011037.

Received 10 JUN 2015
Accepted 14 DEC 2015
Accepted article online 18 DEC 2015
Published online 22 JAN 2016

1. Introduction

On 23 July 2013, a Gulf of Mexico (GoM) petroleum platform owned by Hercules Offshore and operated by Walter Gas and Oil Inc. developed a gas leak. Subsequently, the platform ignited and 44 workers were safely evacuated. The platform, *Hercules 265*, was severely damaged but the well appeared to self-seal. It was finally sealed when a relief well closed the well bore. The *Hercules 265* rig, mat-supported, cantilevered jack-up platform, was not in production at the time of the fire but drilling was ongoing to prepare the rig to resume operations. The site is located 86 km south of the Louisiana Coast in 47 m water depth on the continental shelf, in production block "South Timbalier #220" (Figure 1). Overflights (undertaken by Ms. Bonny Schumaker, On Wings of Care, Inc., and the U.S. Coast Guard) documented a slick or sheen of hydrocarbons releasing from the burning rig running roughly SE. The source of these hydrocarbons is unknown but may have been natural gas condensate, residual liquid oil from the well, or refined oil products released from the well deck. Because there was evidence of liquid hydrocarbons being released into the water and burning of hydrocarbons from the damaged rig, there was concern as to the fate of these hydrocarbons and that they may be transported to the sediments and assimilated by fish in this relatively shallow area.

Comparatively few published studies have documented the impacts of oil and gas production on sediments or fishes in the near-field surrounding active platforms [*Kennicutt II*, 1996a, 1996b; *McDonald et al.*, 1996; *Balk et al.*, 2011]. The studies most relevant to the *Hercules 265* event were conducted in the early 1990s at three natural gas wells in the western GoM, off Texas [*Peterson et al.*, 1996; *Kennicutt II*, 1996a]. In these studies, intensive sampling of water, sediments, invertebrates, and fishes was performed to understand the near-field toxicology associated with gas production facilities. For sediments, the main conclusions were that elevated polycyclic aromatic hydrocarbon (PAH) concentrations were localized to within a few hundred

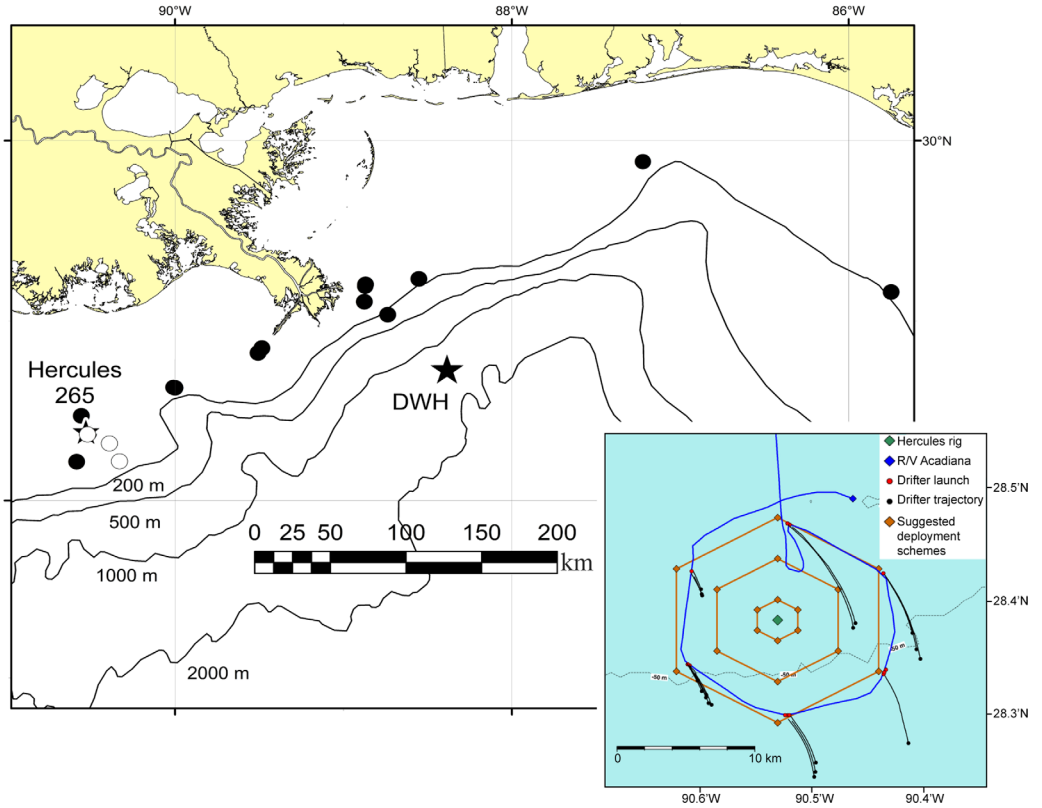

Figure 1. Locations of the *Hercules 265* gas rig, *Deepwater Horizon* oil rig, and sites sampled in 2011–2012 for previous fish studies (black circles) [*McDonald et al*., 1996; *Murawski et al*., 2014]. Insert shows the cruise track of the *R/V Acadiana* during 27–30 July 2013 (blue) with suggested drifter deployment sites (orange), actual drifter deployment locations (red), and drifter trajectories (black) around the *Hercules 265* rig (green).

meters of the rigs, and that sediment particle size showed a trend, of coarser sands nearer the rigs [Kennicutt II, 1996b]. For fishes, comparisons for a number of species were made between the near field (<100 m) versus the far field (>3000 m). Overall, the bile PAH metabolite data from these fish indicated elevated PAH concentrations relative to baseline values suggesting that pollution from unknown sources was occurring [Kennicutt II, 1996b]. However, the fish PAH data did not reveal any interpretable spatial trends relative to the proximity of the rigs (i.e., near-field to far-field differences in PAH levels). This lack of a spatial trend may have been due to the specific fish species analyzed and their ability to move over these limited spatial scales.

Large-scale studies of oil producing regions versus distant control areas have shown that chronic pollution from oil/gas fields can produce a wide variety of sublethal biological effects in fishes [e.g., *Balk et al*., 2011]. While PAHs may only account for a small percent of crude oil mass or are byproducts of combustion of organic matter, they are likely responsible for many of the adverse health and ecological effects observed [*Law and Hellou*, 1999; *Reynaud and Deschaux*, 2006], including potential genotoxic effects [*White et al*., 1999] and/or decrease in abundance of benthic communities [*Montagna et al*., 2013; *Schwing et al*., 2015].

The purpose of this study was to determine the area of potential environmental impact resulting from the *Hercules 265* incident by tracking atmospheric transport of smoke from the burning rig and following the prevailing surface water circulation during 20 days after the blowout. We subsequently analyzed the chemical composition of the sediments, the potential impact to benthic organisms (foraminifera), and the contamination (biliary PAHs) of red snapper (*Lutjanus campechanus*). This species is very abundant and exhibits very limited movements, thus high site fidelity as adults and suitable for contamination studies [*Westmeyer et al*., 2007; *Strelcheck et al*., 2007]. To evaluate hydrocarbon contamination around *Hercules 265*, specifically we measured hydrocarbons including biomarkers (hopanes, steranes) and PAHs in sediments, and PAH metabolites as fluorescent aromatic compounds (FACs) in fish bile, which are a sensitive indicator of recent

PAH exposure in fishes [*Krahn et al*., 1984, 1993, 2005; *Varanasi et al*., 1989]. To provide further assessment of the impacts of the *Hercules 265* blowout, comparisons with data collected in this region prior to and after the *Hercules 265* blowout and data collected elsewhere in the northern GoM in 2013 were conducted.

2. Field Sampling Procedures

A coordinated rapid response to the *Hercules 265* incident [*Joye et al*., 2014] resulted in deployment of surface drifters to track water masses in the vicinity of the Hercules rig following its blowout and to guide the collection of sediment and biological samples for assessment of potential contamination levels. An initial cruise was conducted on 27 July 2013 (4 days after the blowout) with drifters being deployed to follow ocean surface transport over a period of 20 days. A second cruise to the *Hercules 265* site was conducted 36 days after the rig fire was extinguished, to collect environmental samples (sediment, benthic foraminifera, and fishes).

2.1. Deployment of Surface Drifters, 27–30 July 2013 R/V *Acadiana*

Accurate (5 m position uncertainty) and rapid (5–15 min position transmission) data collection from the deployment of clusters of surface drifters are a very reliable method to measure the net surface water transport of all scales of motion on material transport in the ocean [*Haza et al*., 2014; *Poje et al*., 2014]. Our strategy followed hexagonal patterns that provides different options for deployment depending on how close the vessel was permitted to approach the rig, and deployment in triplets for generation of high number of particle pairs to compute dispersion statistics [*Poje et al*., 2014] (Figure 1). On 27 July 2013, 4 days after the fire started, we deployed 20 Lagrangian surface drifters at 60° intervals at a distance of 9.2 km from the *Hercules 265* rig (28.384°N, 90.524°W, Figure 1).

2.2. Sediment and Fish Sampling Cruise on 25 August 2013 R/V *Weatherbird II*

If hydrocarbons were released in sufficient quantities resulting in transport to the sediments, it is likely they would impact benthic habitats and potentially enter the food chain. Aggregation of dispersed oil with minerals and suspended particulate oiled material and its transport to the seafloor has been documented since the 1970s in the *Exxon Valdez* and *Arabian Gulf* oil spills and in laboratory experiments [e.g., *Payne et al*., 2003; *Khelifa et al*., 2005]. This mechanism for oil transport to the sea floor was also documented to have occurred after the *Deepwater Horizon* (DWH) oil spill [*Passow et al*., 2012; *Romero et al*., 2015]. Assuming that petroleum pollution from a point source diminishes/dilutes with distance, our strategy was to test the hypothesis that the pollution level varied inversely with distance from the rig. To do so, on 25 August 2013, we sampled sediment cores at sites located within the potential impacted area by the *Hercules 265* blowout as indicated by the deployed drifters (see section 4), and followed a distance gradient from as close to the rig as we could safely maneuver at 0.2 km (site 1: 28.37°N, 90.52°W; 45 m depth), at 8 km (site 2: 28.32°N, 90.39°W; 54 m depth), and at 18 km (site 3: 28.22°N, 90.33°W; 72 m depth) from the rig. A single, continuous longline fishing gear set at ~0.2 km to a distance of 8 km from the rig was used to collect fishes for analysis of contaminants.

A multicorer (Ocean Instruments MC-800) was used for the collection of sediment cores in order to minimize disturbance of the sediment-water interface during collection. Cores were subsampled in the laboratory at 2 mm (0–20 mm) and 5 mm (>20 mm) intervals. A calibrated threaded rod (one complete turn = 2 mm) was used to extrude the cores, where the sample was then sliced [*Engstrom*, 1993; *Valsangkar*, 2007]. Extruded samples from cores were designated for organic geochemistry (carbon and nitrogen content, carbon stable isotopes, and hydrocarbon analyses) and foraminiferal community analysis. Samples were stored in precombusted glass containers in a freezer (−20°C). Frozen samples for organic geochemistry analysis were freeze dried and ground using a mortar and pestle.

Fish samples were collected following procedures of *Murawski et al*. [2014]. We used a bottom-tending longline, which is an effective sampling technique for demersal species such as red snapper, *L. campechanus*, a dominant component of the fish assemblage in the area surrounding the *Hercules 265* site [*Murawski et al*., 2014]. A 544 kg test mainline was deployed, with 91 kg test leaders, 3.7 m long attached to #13 circle hooks, using cut fish and squid as bait. Hooks were spaced at 18 m intervals along the longline (100 hooks/nm) with a total of 508 hooks deployed. At the beginning and end of the main line, we deployed Star:Oddi© CDST Centi temperature/time/depth recorders to record actual bottom time, as well as bottom temperature

and depth fished. Once the longline was deployed, the vessel steamed back to the start buoy and began haul-back. The soak time of our set was 3 h 39 min. At retrieval, fish species were determined, and fork and total lengths were recorded for each specimen caught. The consecutive hook number of each fish landed was recorded upon retrieval and this number followed the fish through each sampling stage to identify its position along the set. Each specimen was weighed to the nearest g on a Marel© motion-compensated scale, or hand scale (nearest cg) for very large fish. Large sharks (e.g., ~2 m and greater) were photographed for species identification at the rail and released alive. For red snapper, we took bile samples for PAH determinations by dissecting and puncturing the gall bladder and transferring the bile into an amber, prefired 15 × 45 mm vial. Bile samples collected were frozen and stored at −40°C until analysis.

3. Analysis of Collected Data and Samples

3.1. Atmospheric Transport

Given that the *Hercules 265* hydrocarbon release was primarily an atmospheric event, modeling of the associated atmospheric plume was conducted. The University of Miami Unified Wave Interface-Coupled Model (U WIN-CM) was used for real-time prediction of the transport of hydrocarbons in the atmosphere, shortly after the *Hercules 265* rig fire occurred on 23 July 2013. The U WIN-CM is a fully coupled atmosphere-wave-ocean model that has been developed and tested for prediction of the atmosphere-ocean circulation over a broad range of meteorological conditions from calm winds to extreme high winds in winter storms and hurricanes [*Chen et al*., 2013; *Chen and Curcic*, 2015]. The atmospheric model component, Weather and Research and Forecast (WRF) was configured with triply nested grids of 12, 4, and 1.3 km resolution, respectively. The outer domain covered the GoM and West Atlantic region while the inner nests with increased resolution to resolve clouds and fine scale features. The University of Miami Wave Model (UMWM) [*Donelan et al*., 2012] and the Hybrid Ocean Model (HYCOM) are run at 4 km resolution. U WIN-CM was initialized at 0000 UTC daily and forecast for 72 h. A passive tracer was injected at the *Hercules 265* site in the model to represent the plume from the blowout.

Although the high-resolution regional UWIN-CM provides a tool primarily for understanding the atmospheric transport of hydrocarbons at regional scales affected by the synoptic weather systems, the 1.3 km resolution cannot resolve large turbulent eddy circulations (LTECs). In this study, a fourth two-way nested domain with 444 m grid spacing is added in the standard UWIN-CM domain configuration. To further understand the vertical transport of leaked gases at *Hercules 265* site in a typical marine boundary layer (MBL) capped by a sharp inversion and the impact of shallow cumuli (that existed during the *Hercules 265* blowout) on the vertical transport processes in MBL, two different large eddy simulations (LESs) are conducted in this study. One is the classic idealized LES that uses periodic lateral boundary conditions and is initialized and forced by the prescribed profiles based on the UWIN-CM simulations. The other is the hindcasting nested Weather Research & Forecasting (WRF) LES, whose lateral and surface boundary conditions are directly updated from the UWIN-CM simulations through downscaling [*Zhu et al*., 2010; *Zhu*, 2008]. While the former is easy to control, the latter can realistically include the inhomogeneity of surface condition and large-scale forcing as the background field evolves. WRF-LES contains three subdomains with a nesting ratio of 1/3 (Figure 2). The outmost domain is one-way forced by the UWIN-CM simulation at a horizontal resolution of 1.3 km, whereas the two inner domains are two-way nested. The innermost domain of WRF-LES has a horizontal resolution of 49.4 m with 86 levels in the vertical in which 40 levels below 2 km. This is a much higher vertical resolution than that used by the UWIN-CM in which there are 36 levels in the vertical. The WRF-LES is executed for 24 h starting from 12:00 UTC 24 July 2013.

The idealized LES, which is performed by the System of Atmospheric Modeling (SAM) [*Zhu and Zuidema*, 2009], aims to investigate the impact of shallow cumuli on the vertical transport in the MBL. SAM-LES is initialized with the mean vertical profiles of water vapor mixing ratio, potential temperature, and horizontal wind components of the innermost domain of UWIN-CM. The SAM-LES has a horizontal grid-mesh of 640 points in the west-east direction and 160 points in the south-north direction with a grid spacing of 50 m equivalent to that of WRF-LES. In order to better resolve the shallow cumuli at the top of the MBL, SAM-LES has 176 levels below 3510 m with a vertical resolution of 20 m in the vicinity of the MBL inversion. This is a much higher vertical resolution that that of WRF-LES. The idealized SAM-LESs are executed for 12 h and tracers are released 3 h later after the start of the simulation to allow for a sufficient model spin-up.

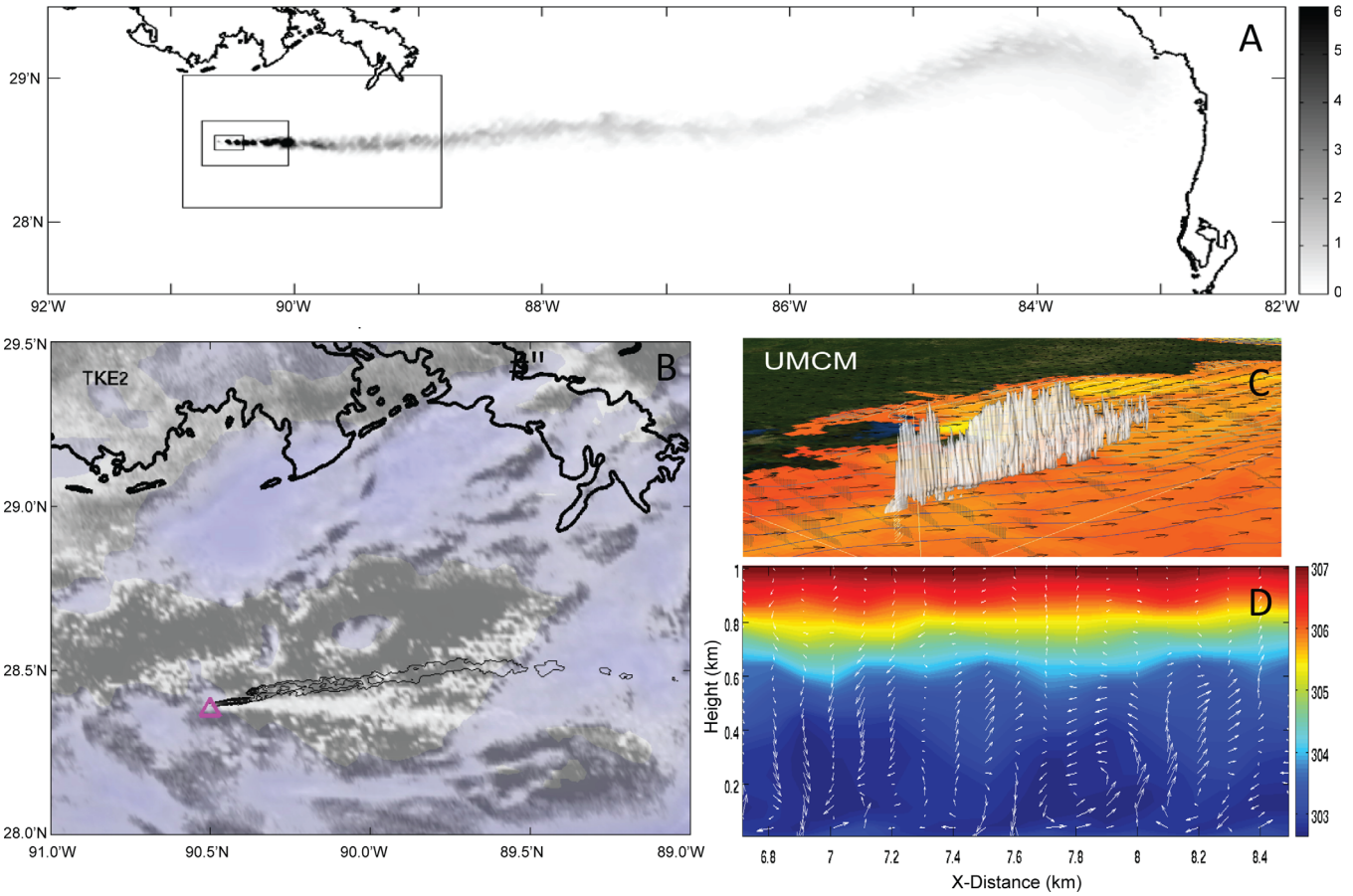

Figure 2. Atmospheric *Hercules 265* rig plume: (a) domain configuration of WRF-LES with respect to UWIN-CM; (b) verification of UWIN-CM forecast of tracer concentration (black contour) and satellite visible and infrared composite images (white shading for the smoke plume) on 24 July 2013 at 21:32 UTC; (c) UWIN-CM forecast of tracer concentration (white), sea surface temperature (color), and surface wind (black vectors) during *Hercules 265* rig fire; and (d) example of vertical structure of the simulated LTECs by WEF-LES overlapped with potential temperature.

3.2. Ocean Surface Transport

Launching a cluster of surface drifters provides a means of tracking material transport and for enhancing our knowledge about the physical oceanography in the GoM, particularly on what scales of motion control near-surface transport in the region. It has been shown that mesoscale motions predominate in the interior of the GoM [*Olascoaga et al*., 2013] while submesoscale motions seemed to prevail within the DeSoto Canyon [*Poje et al*., 2014]. The drifters deployed for the *Hercules 265* incident provide a data set from different geographical locations that allows learning regional distinct transport characteristics in the GoM.

A deeper insight into the Lagrangian circulation in this region can be achieved by isolating the sets of fluid trajectories that act as skeletons of patterns acquired by the fluid transported by the flow. These are widely referred to as Lagrangian Coherent Structures or LCS [*Haller and Yuan*, 2000]. Here the state-of-the-art geodesic theory of LCS is employed [*Haller and Beron-Vera*, 2012; *Beron-Vera et al*., 2013; *Haller and Beron-Vera*, 2013; *Farazmand et al*., 2014]. LCSs are computed using ocean currents inferred from satellite altimetric measurements of sea surface height [*Fu et al*., 2010]. Satellite altimetry observations are not direct and accurate measurements of the ocean's surface velocity field [*Chavanne and Klein*, 2010], but they do provide a good estimation of the mesoscale field [*Fu et al*., 2010]. We explored how much of the Lagrangian circulation in this region can be explained by mesoscale currents like in *Olascoaga et al*. [2013].

Two types of LCS are considered and their effect on the motion of the surface drifters. LCS of the first type is of hyperbolic nature and has the property of attracting nearby fluid trajectories. These were computed as fluid curves embedded in strips of fluid within which the leading-order change in averaged Lagrangian shear is negligible [*Farazmand et al*., 2014]. LCS of the second type is of elliptic nature and define optimal

boundaries of Lagrangian eddies capable of preserving coherence for extended periods of time. These are computed as fluid loops embedded in belts of fluid within which the leading-order change in averaged Lagrangian strain is negligible [*Haller and Beron-Vera*, 2013].

3.3. Sediment Analyses

Prior to analysis of organic carbon content (% TOC) and stable isotopic composition (δ^{13}C), inorganic carbon was removed from freeze-dried sediment samples following the method of *Brodie et al*. [2011]. Samples were then placed in Ag capsules and analyzed using a CarloeErba 2500 Series 2 Elemental Analyzer coupled to a ThermoFinningan Delta XL. All samples were analyzed in duplicate and data reported as the average (<1% difference between duplicates). The results are reported using conventional delta notation in per mil (‰) units relative to the Vienna Pee Dee Belemnite (VPDB) standard. The precision for replicate analyses of external standards (NIST 8573, NIST 8574, and NIIST 1570) was 0.3‰ for δ^{13}C.

Sediment samples were extracted for hydrocarbon quantification using modified EPA methods and QA/QC protocols (8270D, 8015C). Freeze-dried subsamples were spiked with perdeuterated PAHs (d_{10}-acenaphthene, d_{10}-phenanthrene, d_{10}-fluoranthene, d_{12}-benz(*a*)anthracene, d_{12}-benzo(*a*)pyrene, d_{14}-dibenz(*ah*)anthracene, and d_{14}-benzo(*ai*)perylene) and cholastane (d_4-cholestane 2,2,4,4) before extraction. Subsamples were extracted under high temperature (100°C) and pressure (1500 psi) with a solvent mixture 9:1 v:v dichloromethane:methanol (MeOH) using an Accelerated Solvent Extraction system (ASE 200®, Dionex). Activated cu (40 mesh, 99.9%, Sigma-Aldrich, USA) was added to desulfurize each sample extract. Lipid fractions were separated using solid-phase extraction (SPE) with silica/cyanopropyl glass columns (SiO_2/C_3-CN, 1 g/0.5 g, 6 mL). Silica gel (high-purity grade, 100–200 mesh, pore size 30 Å, Sigma-Aldrich, USA) was combusted (450°C for 4 h) and deactivated (2%) previous to assemble the columns. Ultra-clean silica bonded cyanopropyl (C_3-CN, 50 μM, Interchim, USA) was used as well to improve separation of lipid fractions. Lipid fractions were collected by sequentially eluting the extracts with hexane (100%) to collect biomarkers, and hexane/dichloromethylene mixture (3:1, v:v) to collect PAHs. Two extraction blanks were included with each set of samples (10–15 samples).

Biomarkers (hopanes and steranes) were quantified using GC/MS/MS multiple reaction monitoring (MRM) on a Varian 320 triple quadrupole MS. Chromatographic separation of biomarker compounds was conducted using a RXi®5sil column (30 m × 0.25 mm × 0.25 μm) with a GC oven temperature programming of 80°C held for 1 min, then increased to 200°C at a rate of 40°C/min, to 250°C at 5°C/min, to 300°C at 2°C/min, to 320°C at 10°C/min, and held for 2 min. The GC was operated in constant-flow mode (1 mL/min) with an inlet temperature of 275°C and a transfer line temperature of 320°C. Ion source temperature was 180°C and source electron energy was 70 eV. Splitless injections of 1 μL of the sample were conducted. Mass transitions targeted appropriate parent molecular ion masses on Q1 and monitored mass 191.2 (hopanes) or 217.0 (steranes) on Q3, with collision energy held at 10 V throughout. An additional transition (376.7–221) was monitored to quantify the internal standard (d_4-cholestane 2,2,4,4). Ar at a pressure of 1 mtorr was used as a collision gas. Concentrations of biomarkers compounds were calculated using response factors by comparison with a known standard mixture and the internal standard. When no commercial reference standard was available, compounds were quantitated using the response factor for the nearest available homologue in the same compound class. Biomarker compounds are expressed as sediment dry weight concentrations. Recoveries from spiked samples were generally within QA/QC criteria of 90–100%. Procedural blanks processed with each batch of samples were found to be free of contamination. The precision of the analytical method used for quantification of biomarker compounds was evaluated by analyzing the standard reference material NIST 2779 (MC252 crude oil). The determined values ranged between 95% and 100% of the certified values; while in terms of repeatability, the relative standard deviation was below 20%.

Quantification of PAHs was achieved in a gas chromatograph/mass spectrometric detector (GC/MS) in full scan mode (*m/z* 50–550). Splitless injections of 1 μL of the sample were conducted. A RXi®5sil column was used with a GC oven temperature programming of 60°C held for 8 min, then increased to 290°C at a rate of 6°C/min and held for 4 min, then increased to 340°C at a rate of 14°C/min, and held at the upper temperature for 5 min. The temperature of the MS detector was 250°C. Target low molecular weight PAH compounds (LMW PAHs) were naphthalene (N), acenaphthylene (ACL), acenaphthene (ACE), fluorene (F), dibenzothiophene (D), phenanthrene (P), anthracene (AN), and their alkylated homologues. Target high molecular weight PAH compounds (HMW PAHs) were fluoranthene (FL), pyrelene (Pe), pyrene (PY),

benz[*a*]anthracene (B*a*A), chrysene (C), benzo[*b*]fluoranthene (B*b*F), benzo[*k*]fluoranthene (B*k*F), benzo[*a*]-pyrene (B*a*P), dibenz[*a*,*h*]anthracene (D*a*A), indeno[1,2,3-*cd*]pyrene (ID), benzo[*ghi*]perylene (BGP), and their alkylated homologues. Also, we defined carcinogenic PAHs (B*a*A, B*a*P, B*b*F, D*a*A, and ID) as those HMW PAHs known to be carcinogens for animal and probably human based on the U.S. Department of Health and Human Services (HHS) and the U.S. Environmental protection Agency (EPA), respectively [*Agency for Toxic Substances and Disease Registry*, 1995]. Concentrations were calculated using response factors by comparison with a known standard mixture (16-unsubstituited EPA priority and selected isomers: Ultrascientific US-106N PAH mix, NIST 1491a). When no commercial reference standard was available, compounds were quantitated using the response factor for an isomer. Therefore, the concentrations determined for many of the alkylated PAHs were semiquantitative. Aromatic compounds are expressed as sediment dry weight concentrations. Recoveries from spiked samples were generally within QA/QC criteria of 60–114%. Some of the procedural blanks processed with each batch of samples (about 50%) were found to contain background levels or less of some compounds (two-ring and three-ring PAHs) that ranged from 0.1 to 0.6 ng/g. The precision of the analytical method used for quantification of PAHs was evaluated by analyzing the standard reference material NIST 2779 (MC252 crude oil). The determined values ranged between 90 and 98% of the certified values, while in terms of repeatability the relative standard deviation was below 20%.

Replicate hydrocarbon analyses were done in selected samples from the cores collected. Our depth resolution of the core samples allowed us to replicate hydrocarbon analyses at only a few depth intervals, where enough material was available. Confidence intervals (CI) of replicates (N = 3) for biomarkers analysis were 32.5, 38.5, and 41.8 ng g^{-1} for surface layers from site 1, 2, and 3, respectively. CI values for replicates from deeper layers in the cores (20–25 mm) were 18.0, 10.5, and 2.9 ng g^{-1} from site 1, 2, and 3, respectively. CI of replicates (N = 3) for PAH analysis were 19.0, 18.5, and 22.1 ng g^{-1} for surface layers from site 1, 2, and 3, respectively. CI values for replicates from deeper layers in the cores (20–25 mm) for PAHs were 13.0, 26.4, and 3.1 ng g^{-1} from site 1, 2, and 3, respectively. All CI values of replicates were found lower than the variability observed in concentration from surface sediment layers to downcore in all sites (see Results section).

3.4. Foraminifera Sample Preparation and Analysis

Extruded sediment samples for foraminifera analysis were weighed and washed with a sodium hexametaphosphate solution through a 63 μm sieve to disaggregate detrital particles from foraminiferal tests. The fraction remaining on the sieve (>63 μm) was dried in an oven at 32°C for 12 h, weighed again, and stored at room temperature. Individuals from every other depth interval from the upper 25 mm of each core were identified to the species-level and counted (total of 75 samples; 23,817 individual foraminifera).

Total foraminiferal density values were reported in individual per unit volume (number/cm^3) [*Sen Gupta et al*., 2009; *Scott and Medioli*, 1980; *Osterman*, 2003; *Rowe and Kennicutt*, 2009]. Density values were normalized to the known wet volume of each sample based on the diameter of the core tube (10 cm) and the height of each sample (4 or 10 mm). Fisher's Alpha index (a measure of species richness) was used to characterize faunal variability [*Hammer and Harper*, 2006] between the most recently deposited sediments (0–8 mm) and downcore intervals (8–25 mm), as well as between sites with distance from the *Hercules 265* rig.

3.5. Fish Analyses

Twenty-two of the 26 red snapper caught on the longline produced sufficient bile for analysis (in two cases, only the fish heads were retrieved, and in two others, the fish had insufficient volume of bile for analysis). Individual fish bile samples were analyzed for metabolites of PAHs using a semiquantitative high-performance liquid chromatography/fluorescence (HPLC-F) method [*Krahn et al*., 1984, 2005]. This method results in the estimation of relative concentrations of classes of PAH metabolites fluorescing in the regions typified by naphthalene and alkylated homologues (NPH), phenanthrene alkylated homologues (PHN), and benzo[*a*]pyrene (B*a*P). Bile was injected directly onto an Agilent high-performance liquid chromatography/fluorescence system equipped with a C-18 reverse-phase column (following *Murawski et al*. [2014] for methods). The PAH metabolites were eluted with a linear gradient from 100% water (containing a trace amount of acetic acid) to 100% methanol at a flow of 1.0 mL/min. Chromatograms were recorded at the following wavelength pairs: (1) 292/335 nm where many two to three benzene ring aromatic compounds (e.g., NPH) fluoresce, (2) 260/380 nm where several three-ring to four-ring compounds (e.g., PHN) fluoresce, and (3) 380/430 nm where four-ring to five-ring compounds (e.g., B*a*P) fluoresce. Peaks eluting between 6 and 19 min were integrated and the areas of these peaks were summed. The concentrations of fluorescent PAHs in

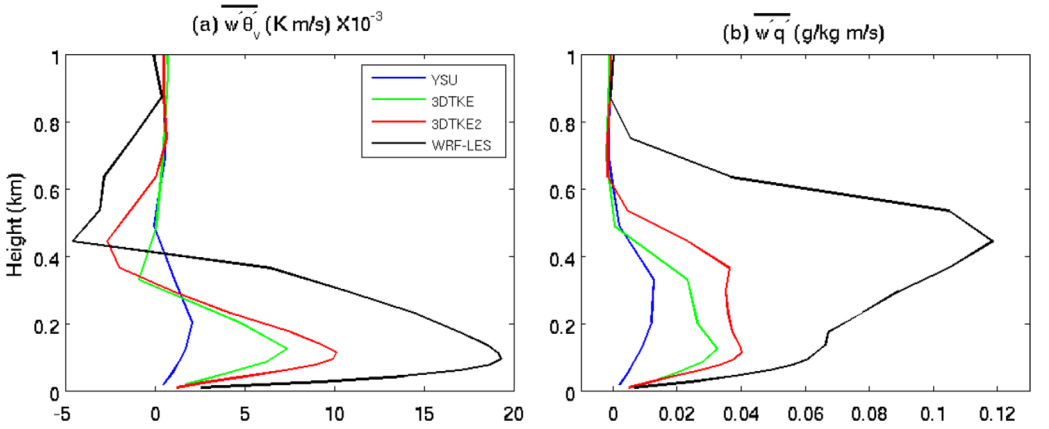

Figure 3. The vertical profiles of (a) buoyancy flux and (b) total water flux at 5:30 UTC 25 July from the UWIN-CM simulations and WRF-LES. "YSU" indicates the UWIN-CM simulation that uses YSU PBL scheme and has a resolution of 1.33 km; "3DTKE" denotes the UWIN-CM simulation that uses a 3-D TKE turbulent mixing scheme and has a resolution of 444 m. "3DTKE2" is exactly the same as "3DTKE" except that the UWIN-CM standard 36 vertical levels are increased to 71 levels. "WRF-LES" indicates the resolved fluxes determined directly from the model output using an eddy correlation method.

the bile samples were determined using NPH, PHN, and B*a*P as external standards and converting the fluorescence response of bile to NHP (ng NPH eq g^{-1} bile), PHN (ng PHN eq g^{-1} bile), or B*a*P (ng B*a*P eq g^{-1} bile) equivalents. Quality assurance was monitored through an interlaboratory comparison between Mote Marine Laboratory and the Northwest Fisheries Science Center, methanol solvent blanks run prior to every sample, samples run in duplicates, and by analysis of calibration standards of NPH, PHN, and B*a*P every 12 samples. CV for replicated samples were $<$15%.

We used linear regression to test for distance effects of PAH contamination, and one-way analysis of variance to test adjacent years for differences in FAC levels between the *Hercules 265* samples and those from the northern GoM taken in 2011 and 2012 [*Murawski et al*., 2014]. Where the assumption of normality of data was rejected, we substituted a Wilcoxon's Ranked Sum Test.

4. Results and Discussion

4.1. Tracking the Atmospheric *Hercules* Plume

The atmospheric plume predictions from the UWIN-CM were evaluated using a satellite image of visible and infrared bands taken 2 days after the *Hercules 265* fire. UWIN-CM predicted an eastward propagation of the atmospheric plume, which is in agreement with the satellite image (Figure 2). Being so close to the surface of the water, the plume is affected by marine boundary layer (MBL) dynamics. Further analysis was conducted by computing LTECs from WRF-LES (Figure 2). The LTECs are constrained by the thickness of the MBL, which varies from 500 to 800 m depending on the time of the day. The output of WRF-LES allowed for direct computation of the vertical fluxes induced by the LTECs using an eddy correlation method. Vertical profiles of resolved buoyancy fluxes and total water fluxes were compared directly from the output of the innermost domain of WRF-LES at 5:30 UTC 25 July, using an eddy correlation method, and compared with the parameterized fluxes from the UWIN-CM forecast fields of three experiments (Figure 3). The first experiment, which uses the YonSei University (YSU) [*Hong et al*., 2006] planetary boundary layer (PBL) scheme, had a resolution of 1.33 km. The second UWIN-CM experiment, which uses a three-dimensional (3-D) turbulent kinetic energy (TKE) turbulent mixing scheme [*Deardorff*, 1970], had a resolution of 0.44 km. The third UWIN-CM experiment is exactly the same as the second experiment except that the UWIN-CM standard 36 vertical levels are increased to 71 levels. These three experiments are named as YSU, 3DTKE, and 3DTKE2, respectively, hereafter. The comparison indicates that the parameterized fluxes by the YSU experiment substantially underestimate the vertical fluxes. By increasing horizontal resolution to 444 m and doubling model vertical levels, UWIN-CM generates much larger vertical fluxes, but they are still substantially different from the fluxes directly resolved by the WRF-LES. This result suggests that a great portion of vertical flux is contributed by turbulent eddies with scales from 50 to 400 m. Also, WRF-LES has a much higher vertical

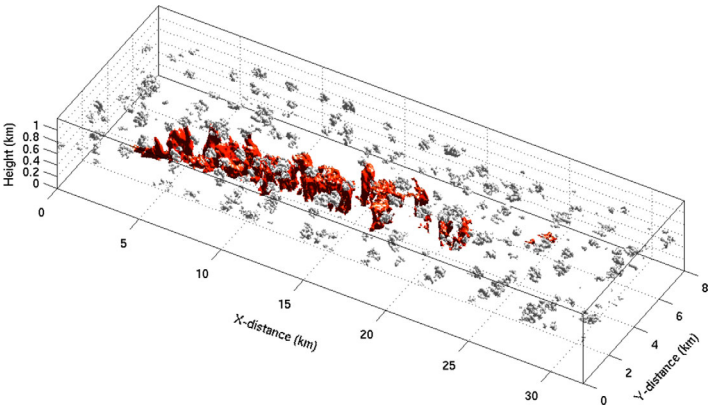

Figure 4. Gas leaking from *Hercules 265* rig in the cloud topped MBL simulated by SAM-LES. The black-red shade indicates the tracer smoke mixing ratio greater than 5.0×10^{-5} g/kg. The well location is at 1.5 km (*x* direction) and 3.5 km (*y* direction) from the coordinate origin. The gray-white shade indicates the cloud water mixing ratio greater than 1.0×10^{-4} g/kg.

resolution than that of UWIN-CM, which indicates that both horizontal and vertical resolution are critical for accurate predictions of vertical transport scalars in the MBL.

Although WRF-LES has a higher vertical resolution than that of UWIN-CM, it may not be sufficient in this case to resolve the fine vertical structure of capping inversion of MBL. The focus of the idealized SAM-LES is on understanding the impact of shallow cumuli on the vertical transport of hydrocarbons (treated as passive tracers) in the MBL when capping inversion is better resolved. The simulated tracer plume shows that shallow cumulus convection can substantially affect the vertical transport of tracers (Figure 4), suggesting the importance of shallow cloud processes associated with the strong capping inversion to the vertical transport in the MBL.

4.2. Surface Water Transport

After deployment, all drifters clearly show inertial oscillations moving toward the southeast direction (Figure 5). This surface water transport direction to the southeast as indicated by the drifters is different from the predominant atmospheric advection direction to the east discussed previously (Figure 2). To assess the potential aquatic impact area by the *Hercules 265* blowout, the center of the mass of the cluster was plotted, as well as the instantaneous area covered by the drifters using a concave hull algorithm (Figure 5). This information was used to set the sampling sites for sediment sites (at ~0.2, 8, and 18 km from the rig) and a longline fishing gear (from ~0.2 to 8 km from the rig) in SE direction of the *Hercules 265* rig.

Within the limitation of the altimetry data set, the analysis of the far-field behavior of the drifters using satellite altimeter data shows drifter motion to be quite reasonably tied to the altimetric attracting LCS and constrained as well by the presence of the boundary of an altimetric coherent Lagrangian eddy situated south of the drifter deployment site (Figure 6). The attracting LCS, for instance, stretches and wraps around, but does not penetrate the boundary of the coherent Lagrangian eddy. The drifters tend to follow the attracting LCS and are not seen to traverse the boundary of the coherent Lagrangian eddy, at least over the duration of the drifter trajectory records. Inspection of a more continuous (daily) sequence of snapshots than that shown in Figure 6 reveals that after circulating around the eddy, some of the drifters take an eastern direction following the attracting LCS. These results provide support to the importance of the mesoscale circulation in transporting fluid (along with passive drifting substances and material, such as surface drifters) in deep waters (away from the continental shelves) of the GoM. It must be noted, however, that the daily sequence of snapshots also reveals that some drifters wander about the deployment site without adhering well to the altimetric attracting LCS. Near and over the continental shelf, the submesoscale circulation may acquire importance, which cannot be reliably resolved by satellite altimetric measurements at present spatiotemporal resolution, as it has been recently noted [*Poje et al.*, 2014].

4.3. Chemical Analyses of Sediments

Sediment cores collected at different distances from the rig (site 1 at ~0.2 km, site 2 at 8 km, and site 3 at 18 km) were analyzed to determine differences in chemical content (i.e., % TOC, $\delta^{13}C$, PAHs, hopanes, and steranes) potentially associated with the *Hercules 265* blowout. Our approach was to test the hypothesis that hydrocarbon levels varied inversely with distance from the rig in the most recently deposited sediment material (top 0–8 mm depth interval in all sediment cores).

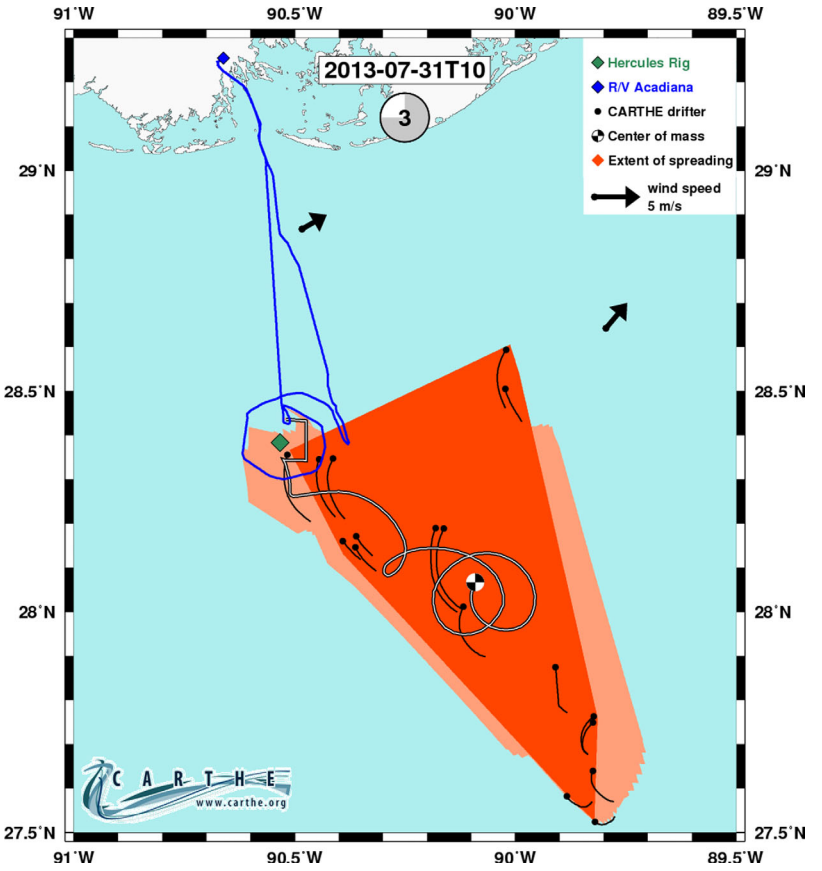

Figure 5. The state of the drifter cluster after 92 h of release. The trajectories have 6 h tails. The center of mass of the cluster shows clear oscillations, SE direction, and southward stretching due to an anticyclonic eddy in the GoM. Dark red marks the instantaneous coverage of the cluster while light red depicts all the regions occupied by the drifters. The arrows show wind data from the NOAA NDBC website (stations SPLL1 and KMDJ). The full evolution of drifter trajectories can be viewed at http://carthe.org/hercules_info/carthe_hercules.mov.

Profiles of carbon content, stable isotopes, and biomarker compounds showed no trend with distance from the well (supporting information Tables S1 and S2; Figure 7). There was a small trend to lighter δ^{13}C values in the surface sediments (0–2 mm) but levels were too low to be related to the spatial trend. Overall, for all sites and all sediment depths, δ^{13}C values were on average $-22.2 \pm 0.9‰$, carbon content averaged $0.9 \pm 0.1\%$, and total biomarker concentrations were 88.2 ± 13.7 ng g^{-1}.

Naphthalene and its alkylated homologues were the most abundant LMW PAHs at site 1 and site 2 ($35 \pm 9\%$ of total PAHs), while phenanthrene and its alkylated homologues were more abundant at site 3 ($14 \pm 4\%$ of total PAHs). However, profiles of LMW PAH concentrations showed no clear trend with distance from the well (supporting information Table S2; Figure 7). In contrast, HMW PAHs (not including perylene) showed a spatial trend only in recent deposited sediment (surface sediment interval <8 mm) with higher values at site 1 (up to 223 ng g^{-1}) followed by site 2 (up to 168 ng g^{-1}) and site 3 (up to 70 ng g^{-1}, but with no clear trend with depth in the sediment; Figure 7). Similarly, perylene was elevated in surface sediments at site 1 (up to 368.1 ng g^{-1}) and site 2 (up to 278.5 ng g^{-1}). Also, fluoranthene, pyrene, and their alkylated homologues increased in surface sediments but only at site 1 (up to 87.3 ng g^{-1}). Carcinogenic PAHs (B*a*A, B*a*P, B*b*F, D*a*A, and ID) showed a trend with distance from the well in surface sediments (<8 mm downcore; Figure 7) with the highest concentrations at site 1 (up to 85.5 ng g^{-1}), intermediate at site 2 (up to 55.6 ng g^{-1}), and lower at site 3 (up to 25.7 ng g^{-1}, with no clear trend with depth). The most abundant carcinogenic PAHs in surface sediments in all sites were ID (up to 31.8 ng g^{-1}), B*b*F (up to 18.2 ng g^{-1}), and B*a*P (up to 9.0 ng g^{-1}) (supporting information Table S1).

The lack of trend with distance from the *Hercules 265* site for hydrocarbons such as biomarkers and LMW PAHs in recently deposited sediments indicates a negligible petrogenic input from the blowout. In contrast, HMW PAHs (including carcinogenic PAHs) decreased with distance from the rig in the surface sediments

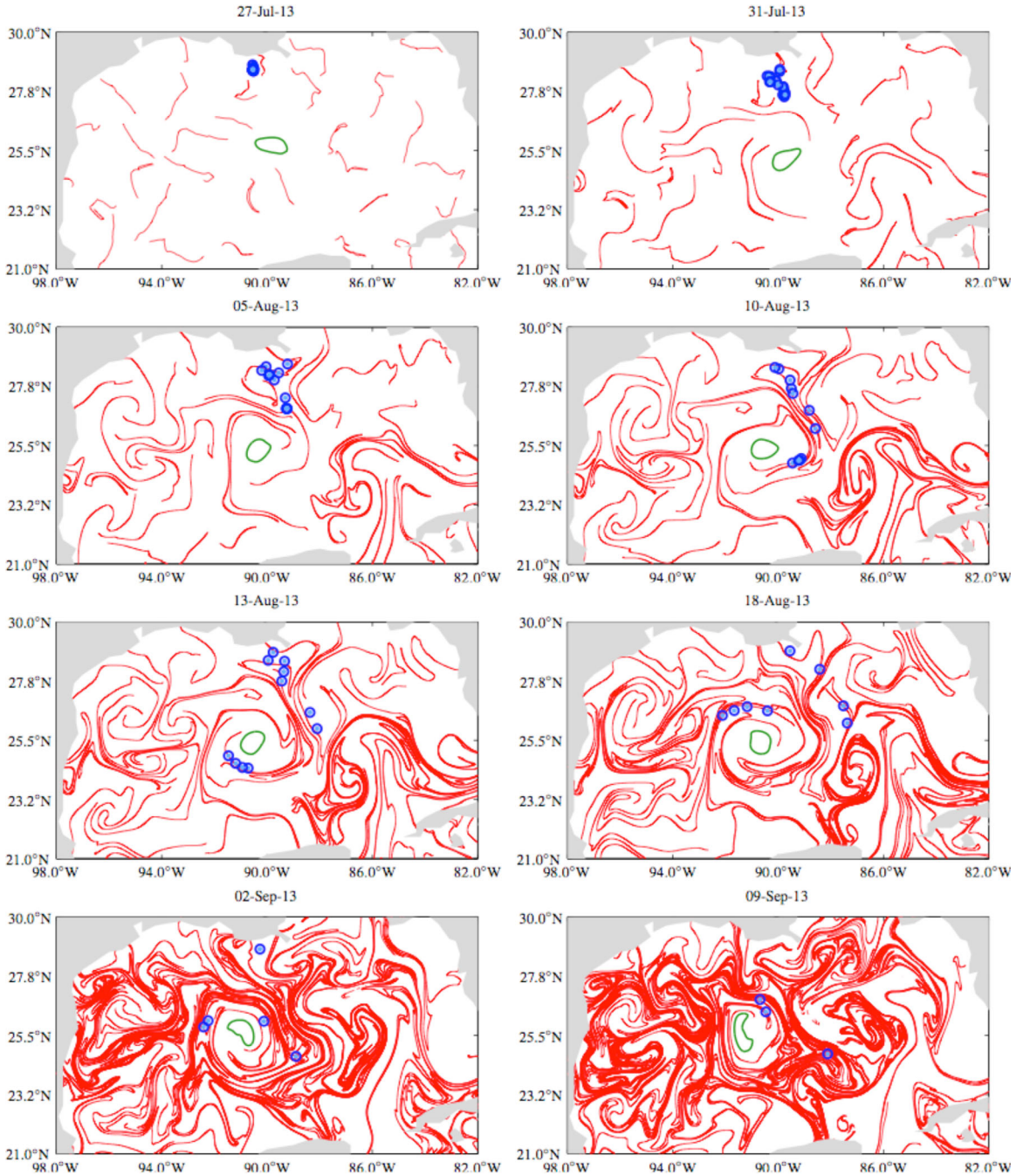

Figure 6. Sequence of selected snapshots of subsequent positions of surface drifters deployed near the *Hercules 265* site (blue dots), the evolution of attracting LCS (red curves), and the boundary of a coherent Lagrangian eddy (green curve) extracted from altimetry-derived currents

indicating higher pyrogenic inputs perhaps associated with the blowout and fire of the rig (supporting information Table S1; Figure 7). Higher HMW PAHs relative to LMW PAHs can also be observed due to weathering processes. For example, biodegradation of oil in the water column during the DWH spill [e.g., *Passow et al*., 2012; *Ziervogel et al*., 2012; *Aeppli et al*., 2014; *Yang et al*., 2014] may have target LMW PAHs as they are more susceptible to microbial degradation [*Douglas et al*., 1996] and modified PAH distribution in deep sediments [*Romero et al*., 2015]. However, they are specific compositional patterns in PAHs that differentiate biodegradation from burn products [*Wang et al*., 1999; *Vane et al*., 2014]. The concentration of chrysene and alkylated homologues were up to 2–3 times higher in the surface sediments, where increased concentrations of four-ring to five-ring PAHs like indeno[1,2,3-*cd*]pyrene were higher than specific LMW

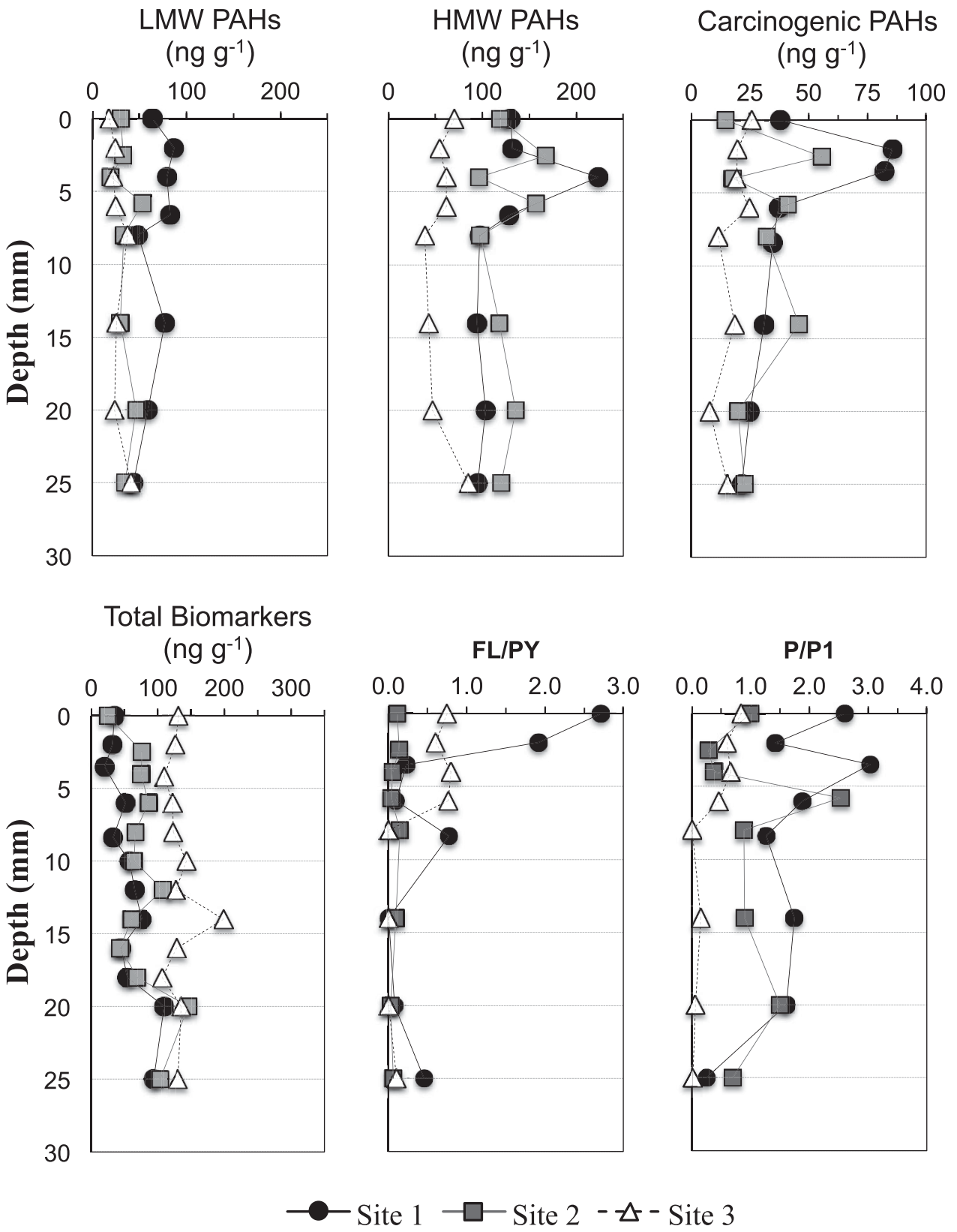

Figure 7. Depth profiles of the total concentration of LMW PAHs (two to three ring), HMW PAHs (four to six ring, without perylene), carcinogens (B*a*A, B*a*P, B*b*F, D*a*A, and ID), and biomarkers (hopanes, steranes, and diasteranes) from sediment cores collected in 2013 at ~0.2 km (site 1), 8 km (site 2), and 18 km (site 3) from the *Hercules 265* rig.

PAH compounds; all indicative of pyrogenic inputs. Another approach to distinguish between petrogenic and pyrogenic PAH inputs to the environment is to calculate diagnostic ratios such as fluoranthene to pyrene and phenanthrene to alkylated homologues (C1–C2 phenanthrene + anthracene), because fluoranthene and phenanthrene are more thermodynamically stable than pyrene and phenanthrene alkylated homologues, respectively [*Sicre et al*., 1987; *Gustafsson and Gschwend*, 1997; *Vane et al*., 2014]. Higher values of these diagnostic ratios at the surface of the sediments (Figure 7) indicate as well that recently deposited PAHs are primarily of a pyrogenic source. Also, a low abundance of alkylated compounds such as 1-methylnaphthalene and 2-methylnaphthalene relative to other PAHs (abundant in diesel fuels, and also found in wood smoke and burnt peatlands) [*Vane et al*., 2014] suggest that noncombusted petroleum sources are an unlikely source in recently deposited PAHs in the studied area. Therefore, our data suggest that surface sediments, especially those close to the Hercules 252 rig, contain primarily pyrogenic PAHs from incomplete combustion of petrogenic sources. However, it should be noted that other weathering process such as evaporation, photodegradation, and dissolution can affect as well the distribution of HMW PAHs in the study area; therefore, results show pyrogenic PAHs modified by the environment.

Human activities such as combustion of organic matter, fossil fuels, natural gas, and surface oil slicks produce pyrogenic PAHs [*Wang et al*., 1999]. In the GoM, pyrogenic PAHs enter the environment predominantly via coastal erosion and to a less extent through the Mississippi River and atmospheric deposition [*Mitra and Bianchi*, 2003; *Overton et al*., 2004]. Previous studies in the GoM have also indicated an increase of HMW PAHs associated with episodic events that were related to human activities (e.g., increase in combustion products) [*Presley et al*., 1998], natural inputs (e.g., hurricanes) [*Mitra et al*., 2009], or both [*Iqbal et al*., 2008]. In 2013, there was no extreme weather condition that may have caused changes in the deposition of pyrogenic PAHs via coastal erosion or the Mississippi River. However, at the blowout site, burnt residues released during and after the fire on the *Hercules 265* may have contaminated the waters close to the rig with pyrogenic PAHs. Once pyrogenic PAHs reached the surface waters may have become rapidly associated with particulate matter and sank to the seafloor southeast of the *Hercules 265* rig as indicated by the drifter trajectories (Figure 5). The strong absorptivity of PAHs to minerals and organic particles [*Radding et al*., 1976; *Luthy et al*., 1997; *Abrajano and Yan*, 2003] has been reported previously to promote sedimentation of spilled oil [*Payne et al*., 2003; *Khelifa et al*., 2005; *Passow et al*., 2012] and likely with the burnt residues produced during in situ burning of oil slick during the *Deepwater Horizon* (DWH) spill [*Romero et al*., 2015].

We also found high concentration of perylene at all depths in the cores at all sites (Table 1). In general, sites 2 and 3 showed little stratigraphic changes in the relative abundance of perylene suggesting a negligible input of perylene from the *Hercules 265* blowout event. However, at site 1 (the location closest to the rig), an increase of perylene concentration in surface sediments (supporting information Table S1) suggests a recent mixed input of PAHs in the aftermath of the *Hercules 265* event. Perylene is found frequently at high concentrations in Louisiana rivers and coastal environments [*Iqbal et al*., 2008] and it is known to be produced by early diagenesis of terrestrial and marine precursors [e.g., *Wang et al*., 1999; *Prahl and Carpenter*, 1979; *Venkatesan*, 1988]. However, it also can be produced during combustion [*Blumer et al*., 1977; *Lipiatou and Saliot*, 1991; *Wang et al*., 1999]. For example, during the combustion of naphthalene, perylene can be produced via cyclodehydrogenation of the binaphthyls [*Howsam and Jones*, 1998]. Therefore, perylene profiles indicate that recently deposited sediments closest to the rig (site 1) may contain perylene from combustion sources, in addition to natural background sources.

Due to predominance of HMW relative to LMW PAHs throughout the cores in all studied sites, we cannot document any significant stratigraphic and spatial changes in the sources of PAH inputs (supporting information Table S1). However, in the surface sediment interval at site 1, we do observe a general twofold increases in the concentration of total HMW PAHs (not including perylene), suggesting that the *Hercules 265* rig could be the source of increasing surface PAHs and, potentially, a continuous source of PAHs to the sedimentary environment even before the blowout. For specific PAHs (i.e., carcinogenic PAHs), we observed increased concentrations in surface sediments at sites 1 and 2 indicating recent inputs in the proximity of the *Hercules 265* rig (supporting information Table S1). Studies on gas rigs off Texas coast also showed pyrogenic inputs from gas exploration activities up to 100–200 m from the gas platforms in the sediments [*Kennicutt II et al*., 1996a, 1996b; *Peterson et al*., 1996].

The *Hercules 265* blowout was a short-term event (2 days) and therefore limited amount of contaminants were released into the environment. Our results are consistent with the short duration of the event, indicating PAH concentrations are lower than levels observed in urbanized and industrialized areas worldwide

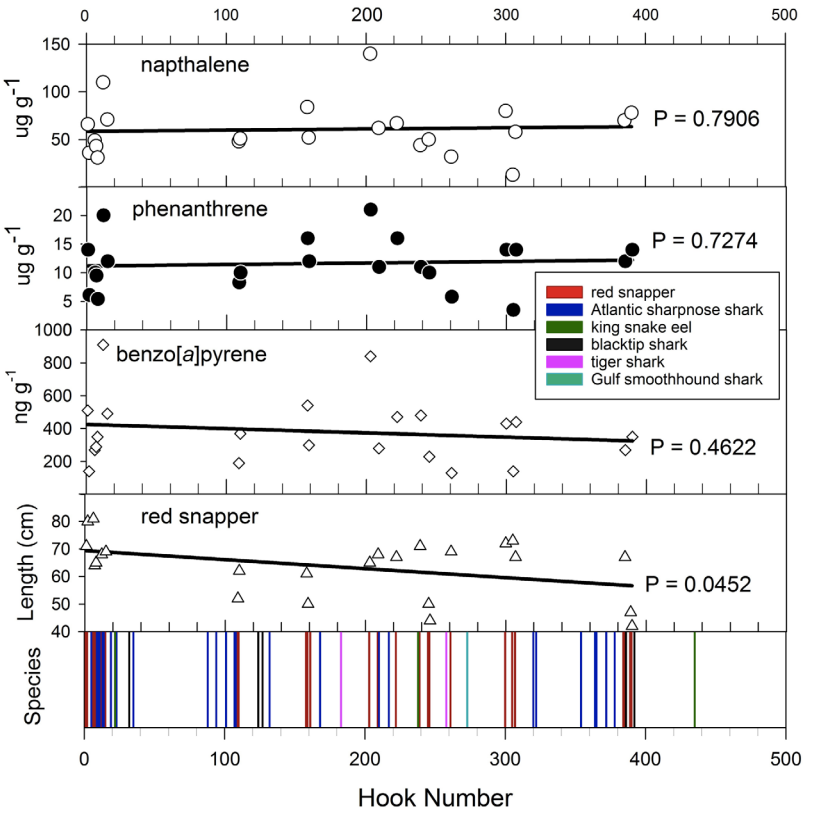

Figure 8. (bottom) Longline sampling catches of six species of fishes caught as a function of hook number ordered from 0.2 to 8 km from the *Hercules 265* gas rig. (top) The bile concentrations of naphthalene (NPH), phenanthrene (PHN), and benzo[*a*]pyrene (B*a*P) metabolite equivalents for each red snapper caught. The fork length of each measurable red snapper caught is also plotted, as are (bottom) the identities of each fish specimen caught by hook number.

[*Qiao et al*., 2006; *Nemr et al*., 2012] and are below established concentrations with potential biological adverse effects [*Long et al*., 1995].

4.4. Benthic Foraminifera

Benthic foraminifera have been used as indicator organisms for pollution [*Alve*, 1995; *Yanko et al*., 1999; *Ernst et al*., 2006; *Denoyelle et al*., 2010] and specifically for petroleum impacts worldwide and in the GoM [*Armynot du Chatelet et al*., 2004; *Brunner et al*., 2013; *Schwing et al*., 2015]. Specifically, *Mojtahid et al*. [2006] found that drilling rigs can affect benthic foraminifera communities by decreasing species richness within a kilometer of the drilling operation. In our study, foraminifera species richness showed a trend with distance from the well (supporting information Table S3) with lower values at site 1 and 2 (9.1 ± 0.6 and 9.9 ± 0.6, respectively) and higher values at site 3 (15.8 ± 0.5). This trend was observed from surface to down core in all sites, suggesting a possible environmental or human induced effect to the benthic environment before *Hercules 265* blowout.

Haynesina germanica has been documented as an indicator of pollution as it outcompetes other taxa in benthic foraminiferal communities that are stressed by PAH pollution [*Armynot du Chatelet et al*., 2004]. In site 1 of our study, the relative abundance of *H. germanica* was significantly higher ($p = 0.0025$) in the most recently deposited sediments (interval 0–8 mm; $6.2 \pm 1.4\%$) compared to downcore values (interval 8–25 mm; $3.1 \pm 1.3\%$) (supporting information Table S3). The 50% increase in the relative abundance of the opportunistic species *H. germanica* at site 1 coincides with increases in HMW and carcinogenic PAH concentrations (Figure 7) indicating a possible short-term effect of the *Hercules 265* blowout.

4.5. Fish Analyses

The longline set caught a total of 64 fishes (Figure 8), consisting of Atlantic sharpnose shark (*Rhizoprionodon terraenovae*, N = 27), red snapper (N = 26), blacktip shark (*Carcharhinus limbatus*, N = 5), king snake eel

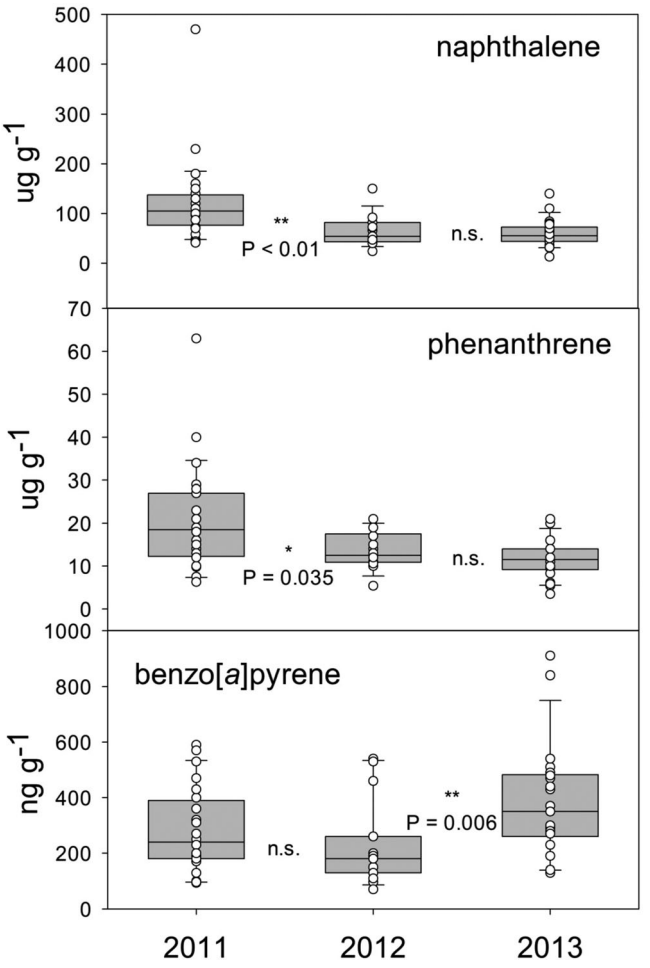

Figure 9. Change in bile concentrations of three PAH metabolites (NPH: naphthalene, PHN: phenanthrene, and B*a*P: benzo[*a*]pyrene) in red snapper sampled in the NGoM from 2011 to 2013. Data for 2013 were obtained from the vicinity of the *Hercules 265* gas rig. Significance (ns = nonsignificant, *significant at $p = 0.05$, and **significant at $p = 0.01$) is indicated between adjacent pairs of years.

(*Ophichthus rex*, N = 3), tiger shark (*Galeocerdom cuvier*, N = 2), and Gulf smoothound (*Mustelus sinusmexicanus*, N = 1). The catch rate was about average for the northern GoM compared to previous reports from 2011 and 2012 of 60 and 67 fishes, respectively [*Murawski et al.*, 2014]. Red snapper was distributed from 0.2 to 8 km SE from the *Hercules 265* rig. The red snapper caught varied in size from 42 to 81 cm, with an average size of 63.5 cm FL (Figure 8). Size declined significantly with distance from the well ($p < 0.05$; using hook number as a proxy for distance; Figure 8).

We tested the hypothesis of a decline in hydrocarbon concentration with distance from the *Hercules 265* site using the concentration of three bile metabolites in red snapper (Figure 8). We chose to focus fish contamination studies on red snapper as a target species because they are relatively sedentary as adults. Numerous studies [e.g., *Westmeyer et al.*, 2007; *Strelcheck et al.*, 2007] have concluded that red snapper exhibit high site fidelity especially over the short 36 day time frame from the beginning of the *Hercules 265* event until our sampling date. Ironically, *Westmeyer et al.* [2007] conducted red snapper site fidelity studies at South Timbalier blocks 128, 134, 135, 151, and 152, about 20 km northeast from the *Hercules 265* site (Figure 1). Their work concluded that red snapper had very high fidelity to individual rigs (about 80%) for a 1 month period. Similarly, *Strelcheck et al.* [2007] in a study that tracked recaptures for over a year found that 86% of their recaptures were within 2 km of the original tagging site. Thus, red snapper seems particularly well suited as a test animal to examine near point-source pollution from petroleum platforms. Interestingly, the fish tagged by *Westmeyer et al.* [2007] were substantially smaller (average fish size 34 cm FL, 36 cm TL) as compared with our fish (average size 63.6 cm FL). In fact, there was little overlap in the size distributions from the two studies (Figure 8). If larger fish on rigs tend to move even less than smaller ones, then their use as sedentary sentinels of pollution is even more appropriate.

Our results indicate that all three FACs showed no trend with distance from the well (Figure 8). The lack of a significant negative relationship between distance from the *Hercules 265* site and LMW PAH uptake probably indicates that petrogenic hydrocarbon pollution from the event (at least as enter the food chain) was minimal and confined to sedimentary surface layers, as suggested as well by the sedimentary profiles of TOC, biomarkers, and LMW PAHs (Figure 7). Likewise, there was no significant difference in NPH and PHN FACs between 2012 and 2013 near the *Hercules 265* site ($p < 0.05$; supporting information Table S3; Figure 9) indicating as well no elevated levels associated with the *Hercules 265* event. However, this finding must be interpreted cautiously because the levels of LMW PAH metabolites were significant lower in 2012 than in 2011 perhaps related to depuration following the DWH episode [*Murawski et al.*, 2014]. A site sampled NW of

Hercules 265 (Stn. 16-150) showed substantially lower levels than at *Hercules 265* in 2013, although the sample size there was small (N = 6; supporting information Table S4).

While LMW PAHs in red snapper apparently did not increase as a result of *Hercules 265*, B*a*P FACs increase significantly ($p = 0.006$) between 2012 and 2013 (Figure 9). Also, there was no significant change between 2011 and 2012 for B*a*P FACs, unlike for LMW PAHs. HMW (B*a*P) FACs increased by a factor of 1.7 (mean) and 1.9 (median) from the 2012 baseline (Table S4). The discrepancy between LMW and HMW results for PAH metabolites is perhaps explained by their origin as discussed previously for the sedimentary record. Many of the HMW PAHs, including B*a*P, are combustion byproducts of hydrocarbons including natural gas (primarily composed of methane) [*Lima et al*., 2005]. The fire on the *Hercules 265* rig was fueled by escaping natural gas and perhaps some refined and unrefined liquid hydrocarbons. It is probable that pyrogenically derived PAHs settled from the atmosphere at the site and were transported in the prevailing SE water mass transport direction (Figure 5), as indicated by our samples. Thus, our results are consistent with a pollution event primarily of pyrogenic PAHs. While the average HMW FACs increased in the 2013 samples over 2012 levels, unlike results for sediments, there was no trend with distance from the rig in the 2013 results. This may be explained by a number of factors including small spatial scale movements of red snapper (e.g., a few hundred meters) or their prey, which include both fishes and benthic invertebrates for these relatively large animals. Alternatively, the source of HMW FACs may have been contact with polluted water moving from NW to SE along the transect sampled.

Data collected adjacent to gas wells in the western GoM [*McDonald et al*., 1996], although not directly comparable to ours, show some important trends (supporting information Table S4). For LWM PAH FACs, levels of naphthalene and phenanthrene in the western GoM were 1.7 and 1.9 times greater than the mean levels at *Hercules 265*, whereas the level of HMW FACs were about 0.5 the levels found at *Hercules 265* (supporting information Table S4). These data reflect different species, but the ratio of LMW to HMW shows that the event of increased HMW FACs associated with *Hercules 265* is not only unusual with respect to the northern GoM but to the western GoM as well, further supporting the argument of increased HMW PAHs as a result of the *Hercules 265* event.

5. Conclusions

The rapid response to the *Hercules 265* blowout on 23 July 2013 demonstrated the feasibility of a multiinstitutional academic collaboration to assess environmental emergencies in the GoM. Two days after the *Hercules 265* blowout, a series of drifters were set to track surface water masses for 20 days and used to guiding the collection of sediment and biological (benthic foraminifera and fishes) samples on 25 August 2013. A geochemical signature of the event was found in SE direction from the *Hercules 265* site in sediment and fish bile samples as shown by elevated levels of HMW PAHs, typical byproduct compounds of combustion. The *Hercules 265* atmospheric plume was transported predominantly to the east and differed in direction to the ocean surface transport which was to the SE. We suggest that HMW PAHs reached the surface waters at the *Hercules 265* site and were transported in SE direction under the influence of a mesoscale anticyclonic eddy until deposition to the seafloor. The levels of contaminants were found to be below established concern concentrations for the environment [*Long et al*., 1995] perhaps due to the short duration of the *Hercules 265* event (~2 days) that limited the amount of contaminants released into the environment.

The *Hercules 265* blowout in 2013 occurred against a backdrop of significant oil pollution on the northern GoM continental shelf from the 2010 DWH spill [*Lubchenco et al*., 2012; *Ylitalo et al*., 2012; *Romero et al*., 2015; *Murawski et al*., 2014] and offshore petroleum production since the 1970s. Monitoring studies in the aftermath of *DWH* provided not only the opportunity to serendipitously sample around the *Hercules 265* as part of a preplanned oceanographic cruise but additionally to gather important baseline contamination levels that were available from the vicinity of *Hercules 265* with which to compare pollution levels caused by the blowout. This scenario emphasizes the importance of an ongoing ocean observing system in the GoM, including routine sampling of waters, sediments, invertebrates and fishes for oil contamination in order to understand the cumulative effects of chronic oil releases, and acute events such as the *DWH* [*Murawski and Hogarth*, 2013] and *Hercules 265*. The fact that the only published information with which to compare *Hercules 265* effects was from a study more than two decades prior to the *Hercules 265* event should serve

notice that such information is seriously out of date relative to developments in the industry (e.g., deeper exploration and enhanced production). Furthermore, because there are multiple chronic, low level releases of hydrocarbons to the GoM [e.g., *Presley et al.*, 1998; *Santschi et al.*, 2001; *Mitra and Bianchi*, 2003; *Kvenvolden and Cooper*, 2003; *Ocean Studies Board and Marine Board, National Research Council*, 2003; *Overton et al.*, 2004; *Iqbal et al.*, 2007; *Murawski et al.*, 2014] resolving the effects of a single event requires broad-based and spatially resolved sampling. Given the frequency of these serious pollution events (e.g., oil spills, gas, and oil blowouts) and others such as hurricanes [*Hom et al.*, 2008], it seems prudent to conduct such baseline studies on a regular basis.

Acknowledgments

This research was supported by a grant from the Gulf of Mexico Research Initiative, through its Center for Integrated Modeling and Analysis of Gulf Ecosystems (C-IMAGE) and the Consortium for Advanced Research on Transport of Hydrocarbons in the Environment (CARTHE) consortia. Data from 2011 were collected under grant NA11NMF4720151, Systematic Survey of Fish Diseases in the Gulf of Mexico, to SAM, from the National Marine Fisheries Service (NMFS), NOAA. Captains and crew of the fishing vessel *Pisces*, and research vessel *Weatherbird II*, operated by the Florida Institute of Oceanography, conducted our longline and sediment sampling. We appreciate the efforts of our field team including A. Wallace, E. Herdter, K. Deak, and S. Gilbert, and lab assistance by N. Zenzola, Q. Miller, and G. Ellis. We thank Chia-Ying Lee for her assistance in tracer analysis in UWIN-CM. We also appreciate the 2011 chemical and data analysis conducted by B. Anulacion, R. Boyer, J. Bolton, J. Herman, P. Hoppe, R. Pearce, and C. Sloan at the NOAA/NMFS Northwest Fisheries Science Center. The 2012 bile analyses were assisted by E. Pulster, Mote Marine Laboratory. Data summarized in this paper from C-IMAGE and CARTHE consortia are available online at https://data.gulfresearchinitiative.org/data/R1.x135.119:0011, and https://data.gulfresearchinitiative.org/data/R1.x134.073:0012/.

References

Abrajano, T. A., and B. Yan (2003), High molecular weight petrogenic and pyrogenic hydrocarbons in aquatic environments, in *Treatise on Geochemistry, Environ. Geochem.*, vol. 9, edited by B. S. Lollar, pp. 475–510, Elsevier, Italy.

Aeppli, C., R. K. Nelson, J. R. Radović, C. Carmichael, D. L. Valentine, and R. M. Christopher (2014), Recalcitrance and degradation of petroleum biomarkers upon abiotic and biotic natural weathering of Deepwater Horizon oil, *Environ. Sci. Technol.*, *48*, 6726–6734, doi: 10.1021/es500825q.

Agency for Toxic Substances and Disease Registry (1995), *Toxicological Profile for Polycyclic Aromatic Hydrocarbons (PAHs)*, Public Health Serv., U.S. Dep. of Health and Hum. Serv., Altanta, Ga.

Alve, E. (1995), Benthic foraminiferal responses to estuarine pollution: A review, *J. Foraminiferal Res.*, *25*(3), 190–203.

Armynot du Chatelet, E., J. P. Debenay, and R. Soulard (2004), Foraminiferal proxies for pollution monitoring in moderately polluted harbors, *Environ. Pollut.*, *127*, 27–40.

Balk, L., et al. (2011), Biomarkers in natural fish populations indicate adverse biological effects of offshore oil production, *PLoS ONE*, *6*(5), e19735, doi:10.1371/journal.pone.0019735.

Beron-Vera, F. J., Y. Wang, M. J. Olascoaga, G. J. Goni, and G. Haller (2013), Objective detection of oceanic eddies and the Agulhas leakage, *J. Phys. Oceanogr.*, *43*, 1426–1438.

Blumer, M., W. Blumer, and T. Reich (1977), Polycyclic aromatic hydrocarbons in soils of a mountain valley: Correlation with highway traffic and cancer incidence, *Environ. Sci. Technol.*, *11*(12), 1082–1084.

Brunner, C. A., K. M. Yeager, R. Hatch, S. Simpson, J. Keim, K. B. Briggs, and P. Louchouarn (2013), Effects of oil from the 2010 Macondo Well Blowout on Marsh Foraminifera of Mississippi and Louisiana, USA, *Environ. Sci. Technol.*, *47*, 9115–9123.

Brodie, C. R., et al. (2011), Evidence for bias in C/N, δ13C and δ15N values of bulk organic matter, and on environmental interpretation, from a lake sedimentary sequence by pre-analysis acid treatment methods, *Quat. Sci. Rev.*, *30*, 3076–3087, doi:10.1016/j.quascirev.2011.07.003.

Chavanne, C. P., and P. Klein (2010), Can oceanic submesoscale processes be observed with satellite altimetry?, *Geophys. Res. Lett.*, *37*, L22602, doi:10.1029/2010GL045057.

Chen, S. S., and M. Curcic (2015), Coupled modeling and observations of ocean surface waves in Hurricane Ike (2008) and Superstorm Sandy (2012), *Ocean Modell.*, doi:10.1016/j.ocemod.2015.08.005, in press.

Chen, S. S., W. Zhao, M. A. Donelan, and H. L. Tolman (2013), Directional wind-wave coupling in fully coupled atmosphere-wave-ocean models: Results from CBLAST-Hurricane, *J. Atmos. Sci.*, *70*, 3198–3215.

Deardorff, J. (1970), A numerical study of three-dimensional turbulent channel flow at large Reynolds numbers, *J. Fluid Mech.*, *41*(2), 453–480.

Denoyelle, M., F. J. Jorissen, D. Martin, F. Galgani, and J. Mine (2010), Comparison of benthic foraminifera and macrofaunal indicators of the impact of oil-based drill mud disposal, *Mar. Pollut. Bull.*, *60*(11), 2007–2021.

Donelan, M. A., M. Curcic, S. S. Chen, and A. K. Magnusson (2012), Modeling waves and wind stress, *J. Geophys. Res.*, *117*, C00J23, doi: 10.1029/2011JC007787.

Douglas, G. S., A. E. Bence, R. C. Prince, S. J. McMillen, and E. L. Butler (1996), Environmental stability of selected petroleum hydrocarbon source and weathering ratio, *Environ. Sci. Technol.*, *38*, 3958–3964.

Engstrom, D. R. (1993), A lightweight extruder for accurate sectioning of soft-bottom lake sediment cores in the field, *Limnol. Oceanogr.*, *38*(8), 1796–1802.

Ernst, S. R., J. Morvan, E. Geslin, A. Le Bihan, and F. J. Jorissen (2006), Benthic foramineral response to experimentally induced Erika oil pollution, *Mar. Micropaleontol.*, *61*, 76–93.

Farazmand, M., D. Blazevski, and G. Haller (2014), Shearless transport barriers in unsteady two-dimensional flows and maps, *Physica D*, *278–279*, 44–57.

Fu, L. L., D. B. Chelton, P. Y. Le Traon, and R. Morrow (2010), Eddy dynamics from satellite altimetry, *Oceanography*, *23*, 14–25.

Gustafsson, O., and P. Gschwend (1997), Soot as a strong partitioning medium for polycyclic aromatic hydrocarbons in aquatic systems, in *Molecular Markers in Environmental Geochemistry*, edited by R. P. Eganhouse, pp. 365–381, Am. Chem. Soc., Washington, D. C.

Haller, G., and F. J. Beron-Vera (2012), Geodesic theory of transport barriers in two-dimensional flows, *Physica D*, *241*, 1680–1702.

Haller, G., and F. J. Beron-Vera (2013), Coherent Lagrangian vortices: The black holes of turbulence, *J. Fluid Mech.*, *731*, R4.

Haller, G., and G. Yuan (2000), Lagrangian Coherent Structures and mixing in two-dimensional turbulence, *Physica D*, *147*, 352–370.

Hammer, O., and D. A. T. Harper (2006), *Paleontological Data Analysis*, Blackwell, Malden, Mass.

Haza, A. C., T. M. Özgökmen, A. Griffa, A. C. Poje, and P. Lelong (2014), How does drifter position uncertainty affect ocean dispersion estimates?, *J. Atmos. Oceanic Technol.*, *31*, 2809–2828.

Hom, T., T. K. Collier, M. M. Krahn, M. S. Strom, G. M. Ylitalo, W. B. Nilsson, R. N. Paranjpye, and U. Varanasi (2008), Assessing seafood safety in the aftermath of Hurricane Katrina, *Am. Fish. Soc. Symp.*, *64*, 73–93.

Hong, S. Y., Y. Noh, and J. Dudhia (2006), A new vertical diffusion package with an explicit treatment of entrainment processes, *Mon. Weather Rev.*, *134*, 2318–2340.

Howsam, M., and K. C. Jones (1998), Sources of PAHs in the environment, in *PAHs and Related Compounds the Hand-Book of Environmental Chemistry*, vol. 3, part I, edited by A. H. Neilson, pp. 138–174, Springer, Berlin.

Iqbal, J., R. J. Portier, and D. Gisclair (2007), Aspects of petrochemical pollution in coastal Louisiana, *Mar. Pollut. Bull.*, *54*, 792–819.

Iqbal, J., E. B. Overton, and D. Gisclair (2008), Polycyclic aromatic hydrocarbons in Louisiana Rivers and coastal environments: Source fingerprinting and forensic analysis, *Environ. Forensics*, *9*, 63–74, doi:10.1080/15275920801888301.

Joye, S. B., J. P. Montoya, S. Murawski, T. M. Özgökmen, T. Wadem, R. Montouro, B. J. Roberts, D. J. Hollander, W. H. Jeffrey, and J. P. Chanton (2014), A rapid response study of the Hercules gas well blowout, *Eos Trans. AGU*, *95*(38), 341–342.
Kennicutt II, M. C., R. H. Green, P. Montagna, and P. F. Roscigno (1996a), Gulf of Mexico Offshore Operations Monitoring Experiment (GOOMEX), Phase I: Sublethal responses to contaminant exposure—Introduction and overview, *Can. J. Fish. Aquat. Sci.*, *53*, 2540–2553.
Kennicutt II, M. C., P. N. Boothe, T. L. Wade, S. T. Sweet, R. Rezak, F. J. Kelly, J. M. Brooks, B. J. Presley, and D. A. Wiesenburg (1996b), Geochemical patterns in sediments near offshore production platforms, *Can. J. Fish. Aquat. Sci.*, *53*(11), 2554–2566, doi:10.1139/f96-214.
Khelifa, A., P. S. Hill, and K. Lee (2005), The role of oil-sediment aggregation in dispersion and biodegradation of spilled oil, in *Oil Pollution and Its Environmental Impact in the Arabian Gulf Region*, edited by M. Al-Azab, W. El-Shorbagy, and S. Al-Ghais, pp. 131–145, Elsevier, Netherlands.
Krahn, M. M., M. S. Myers, D. G. Burrows, and D. C. Malins (1984), Determination of xenobiotics in bile of fish from polluted waterways, *Xenobiotica*, *14*, 633–646.
Krahn, M. M., G. M. Ylitalo, J. Buzitis, J. L. Bolton, C. A. Wigren, S. L. Chan, and U. Varanasi (1993), Analyses of petroleum-related contaminants in marine fish and sediments following the Gulf oil spill, *Mar. Pollut. Bull.*, *27*, 285–292.
Krahn, M. M., G. M. Ylitalo, and T. K. Collier (2005), *Analysis of Bile of Fish Collected in Coastal Waters of the Gulf of Mexico Potentially Affected by Hurricane Katrina to Determine Recent Exposure to Polycyclic Aromatic Compounds (PACs)*, M.S. NOAA, Natl. Mar. Fish. Serv., Northwest Fish. Sci. Cent., Seattle, Wash.
Kvenvolden, K. A., and C. K. Cooper (2003), Natural seepage of crude oil into the marine environment, *Geo-Mar. Lett.*, *23*, 140–146.
Law, R. J., and J. Hellou (1999), Contamination of fish and shellfish following oil spill incidents, *Environ. Geosci.*, *6*(2), 90–98.
Lima, A. L., J. W. Farrington, and C. M. Reddy (2005), Combustion-derived polycyclic aromatic hydrocarbons in the environment—A review, *Environ. Forensics*, *6*(2), 109–131.
Lipiatou, E., and A. Saliot (1991), Fluxes and transport of anthropogenic and natural polycyclic aromatic hydrocarbons in the western Mediterranean sea, *Mar. Chem.*, *32*, 51–71.
Long, E. R., D. D. Macdonald, S. L. Smith, and F. D. Calder (1995), Incidence of adverse biological effects within ranges of chemical concentrations in marine and estuarine sediments, *Environ. Manage.*, *19*, 81–97.
Lubchenco, J., M. McNutt, G. Dreyfus, S. A. Murawski, D. Kennedy, P. Anastas, S. Chu, and T. Hunter (2012), Science in support of the *Deepwater Horizon* response—An introduction, *Proc. Natl. Acad. Sci. U. S. A.*, *109*(50), 20,212–20,221.
Luthy, R. G., G. R. Aiken, M. L. Brusseau, S. D. Cunningham, P. M. Gschwend, J. J. Pignatello, M. Reinhard, S. J. Traina, W. J. Weber, and J. Westall (1997), Sequestration of hydrophobic organic contaminants by geosorbents, *Environ. Sci. Technol.*, *31*, 3341–3347.
McDonald, S. J., K. L. Willett, J. Thomsen, K. B. Beatty, K. Connor, T. R. Narasimhan, C. M. Erickson, and S. H. Safe (1996), Sublethal detoxification responses to contaminant exposure associated with offshore oil production, *Can. J. Fish. Aquat. Sci.*, *53*, 2606–2617.
Mitra, S., and T. S. Bianchi (2003), A preliminary assessment of polycyclic aromatic hydrocarbon distributions in the lower Mississippi River and Gulf of Mexico, *Mar. Chem.*, *82*, 273–288.
Mitra, S., J. J. Lalicata, M. A. Allison, and T. M. Dellapenna (2009), The effects of Hurricanes Katrina and Rita on seabed polycyclic aromatic hydrocarbon dynamics in the Gulf of Mexico, *Mar. Pollut. Bull.*, *58*, 851–857, doi:10.1016/j.marpolbul.2009.01.016.
Mojtahid, M., F. Jorissen, J. Durrieu, F. Galgani, H. Howa, F. Redois, and R. Camps (2006), Benthic foraminfera as bio-indicators of drill cutting disposal in tropical east Atlantic outer shelf environments, *Mar. Micropaleontol.*, *61*, 58–75.
Montagna, P. A., J. G. Baguley, C. Cooksey, I. Hartwell, L. J. Hyde, et al. (2013), Deep-sea benthic footprint of the deepwater horizon blowout, *PLoS ONE*, *8*, e70540, doi:10.1371/journal.pone.0070540.
Murawski, S. A., and W. T. Hogarth (2013), Enhancing the ocean observing system to meet restoration challenges in the Gulf of Mexico, *Oceanography*, *26*(1), 10–16.
Murawski, S. A., W. T. Hogarth, E. Peebles, J. Stein, G. Ylitalo, and L. Barbieri (2014), Prevalence of external skin lesions and PAH concentrations in Gulf of Mexico fishes, Post-*Deepwater Horizon*, *Trans. Am. Fish. Soc.*, *143*(4), 1084–1097.
Nemr, A. El., M. M. El-Sadaawy, A. Khaled, and S. O. Draz (2012), Aliphatic and polycyclic aromatic hydrocarbons in the surface sediments of the Mediterranean: Assessment and source recognition of petroleum hydrocarbons, *Environ. Monit. Assess.*, *185*, 4571–4589, doi:10.1007/s10661-012-2889-1.
Ocean Studies Board and Marine Board, National Research Council (2003), *Oil in the Sea III. Inputs, Fates, and Effects*, Natl. Acad. Press, Washington, D. C.
Olascoaga, M. J., et al. (2013), Drifter motion in the Gulf of Mexico constrained by altimetric Lagrangian Coherent Structures, *Geophys. Res. Lett.*, *40*, 6171–6175, doi:10.1002/2013GL058624.
Osterman, L. E. (2003), Benthic foraminifers from the continental shelf and slope of the Gulf of Mexico: An indicator of shelf hypoxia, *Estuarine Coastal Shelf Sci.*, *58*, 17–35.
Overton, E. B., B. M. Ashton, and M. S. Miles (2004), Historical polycyclic and petroleum hydrocarbon loading in the Northern Central Gulf of Mexico shelf sediments, *Mar. Pollut. Bull.*, *49*, 557–563.
Passow, U., K. Ziervogel, V. Asper, and A. Diercks (2012), Marine snow formation in the aftermath of the Deepwater Horizon oil spill in the Gulf of Mexico, *Environ. Res. Lett.*, *7*, 035301, doi:10.1088/1748-9326/7/3/035301.
Payne, J. R., J. R. Clayton, and B. E. Kirstein (2003), Oil/suspended particulate material interactions and sedimentation, *Spill Sci. Technol. Bull.*, *8*, 201–221, doi:10.1016/S1353-2561(03)00048-3.
Peterson, C. H., M. C. Kennicutt II, R. H. Green, P. Montagna, D. E. Harper Jr., E. N. Powell, and P. F. Roscigno (1996), Ecological consequences of environmental perturbations associated with offshore hydrocarbon production: A perspective on long-term exposure in the Gulf of Mexico, *Can. J. Fish. Aquat. Sci.*, *53*, 2637–2654.
Poje, A. C., et al. (2014), Submesoscale dispersion near the Deepwater Horizon spill, *Proc. Natl. Acad. Sci. U. S. A.*, *111*, 12,693–12,698.
Prahl, G., and R. O. Y. Carpenter (1979), The role of zooplankton fecal pellets in the sedimentation of polycyclic aromatic hydrocarbons in Dabob Bay, Washington, *Geochem. J.*, *43*, 1959–1972.
Presley, B. J., T. L. Wade, P. Santschi, and M. Baskaran (1998), Historical contamination of Mississippi River Delta, Tampa Bay and Galveston Bay sediments, *NOAA Tech. Memo. NOS ORCA 127*, 136 pp., NOAA, Md.
Qiao, M., C. Wang, S. Huang, D. Wang, and Z. Wang (2006), Composition, sources, and potential toxicological significance of PAHs in the surface sediments of the Meiliang Bay, Taihu Lake, China, *Environ. Int.*, *32*, 28–33.
Radding, S., T. Mill, C. Gould, D. Liu, H. Johnson, D. Bomberger, and C. Fojo (1976), *The Environmental Fate of Selected Polynuclear Aromatic Hydrocarbons*, EPA, Washington, D. C.
Reynaud, S., and P. Deschaux (2006), The effects of polycyclic aromatic hydrocarbons on the immune system of fish: A review, *Aquat. Toxicol.*, *77*, 229–238.

Romero, I. C., P. T. Schwing, G. R. Brooks, R. A. Larson, D. W. Hastings, E. Greg, E. A. Goddard, and D. J. Hollander (2015), Hydrocarbons in deep-sea sediments following the 2010 *Deepwater Horizon* blowout in the Northeast Gulf of Mexico, *PLoS ONE*, *10*(5), e0128371, doi: 10.1371/journal.pone.0128371.

Rowe, G. T., and M. C. Kennicutt II (2009), Northern Gulf of Mexico Continental Slope Habitats and Benthic Ecology Study: Final Report, *OCS Study MMS 2009-039*, 456 pp., U.S. Dep. of the Inter., Miner. Manage. Serv., Gulf of Mexico OCS Reg., New Orleans, La.

Santschi, P. H., B. J. Presley, T. L. Wade, B. Garcia-Romero, and M. Baskaran (2001), Historical contamination of PAHs, PCBs, DDTs, and heavy metals in Mississippi River Delta, Galveston Bay and Tampa Bay sediment cores, *Mar. Environ. Res.*, *52*, 51–79.

Schwing, P. T., I. C. Romero, G. R. Brooks, D. W. Hastings, R. A. Larson, and D. J. Hollander (2015), A decline in deep-sea benthic foraminifera following the deepwater horizon event in the Northeastern Gulf of Mexico, *PLoS ONE*, *10*(3), e0120565, doi:10.1371/journal.pone.0120565.

Scott, D. B., and F. S. Medioli (1980), Living vs. total foraminiferal populations: Their relative usefulness in paleoecology, *J. Paleontol.*, *54*, 814–831.

Sen Gupta, B. K., M. K. Lobegeier, and L. E. Smith (2009), Foraminiferal communities of bathyal hydrocarbon seeps, northern Gulf of Mexico: A taxonomic, ecologic, and geologic study, *OCS Study MMS 2009-013*, 385 pp., U.S. Dep. of the Inter., Miner. Manage. Serv., Gulf of Mexico OCS Reg., New Orleans, La.

Sicre, M. A., J. C. Marty, A. Saliot, X. Aparicio, J. Grimalt, and J. Albaiges (1987), Aliphatic and aromatic hydrocarbons in different sized aerosols over the Mediterranean Sea; occurrence and origin, *Atmos. Environ.*, *21*, 2247–2259.

Strelcheck, A. J., J. H. Cowan Jr., and W. F. Patterson III (2007), Site fidelity, movement, and growth of red snapper: Implications for artificial reef management, *Am. Fish. Soc. Symp.*, *60*, 147–162.

Valsangkar, A. B. (2007), A device for finer-scale sub-sectioning of aqueous sediments, *Curr. Sci.*, *92*(4), 5–8.

Vane, C. H., A. W. Kim, D. J. Beriro, M. R. Cave, K. Knights, V. Moss-Hayes, and P. C. Nathanail (2014), Polycyclic aromatic hydrocarbons (PAH) and polychlorinated biphenyls (PCB) in urban soils of Greater London, UK, *Appl. Geochem.*, *51*, 303–314.

Varanasi, U., J. E. Stein, and M. Nishimoto (1989), Biotransformation and disposition of polycyclic aromatic hydrocarbons (PAH) in fish, in *Metabolism of Polycyclic Aromatic Hydrocarbons in the Aquatic Environment*, edited by U. Varanasi, CRC Press, Boca Raton, Fla.

Venkatesan, M. I. (1988), Occurrence and possible sources of perylene in marine sediments: a review, *Mar. Chem.*, *25*, 1–27.

Wang, Z., M. Fingas, Y. Y. Shu, L. Sigouin, M. Landriault, P. Lambert, R. Turpin, P. Campagna, and J. Mullin (1999), Quantitative characterization of PAHs in burn residue and soot samples and differentiation of pyrogenic PAHs from petrogenic PAHs: The 1994 Mobile Burn Study, *Environ. Sci. Technol.*, *33*, 3100–3109, doi:10.1021/es990031y.

Westmeyer, M. P., C. A. Wilson III, and D. L. Neiland (2007), Fidelity of red snapper to petroleum platforms in the northern Gulf of Mexico, *Am. Fish. Soc. Symp.*, *60*, 105–121.

White, P. A., S. Robitaille, and J. B. Rasmussen (1999), Heritable reproductive effects of benzo[*a*]pyrene on the fathead minnow (*Pimephales promelas*), *Environ. Toxicol. Chem.*, *18*(8), 1843–1847.

Yang, T., L. M. Nigro, T. Gutierrez, L. D'Ambrosio, S. B. Joye, H. Raymond, and A. Teske (2014), Pulsed blooms and persistent oil-degrading bacterial populations in the water column during and after the Deepwater Horizon blowout, *Deep Sea Res., Part II*, 1–10, doi:10.1016/j.dsr2.2014.01.014.

Yanko, V., J. J. Arnold, and W. C. Parker (1999), Effects of marine pollution on benthic foraminifera, in *Modern Foraminifera*, edited by B. Sen Gupta, pp. 217–235, Kluwer Acad., Boston, Mass.

Ylitalo, G. M., et al. (2012), Federal seafood safety response to the *Deepwater Horizon* oil spill, *Proc. Natl. Acad. Sci. U. S. A.*, *109*(50), 20,274–20,279.

Zhu, P. (2008), Simulation and parameterization of the turbulent transport in the hurricane boundary layer by large eddies, *J. Geophys. Res.*, *113*, D17104, doi:10.1029/2007JD009643.

Zhu, P., and P. Zuidema (2009), On the use of PDF schemes to parameterize sub-grid clouds, *Geophys. Res. Lett.*, *36*, L05807, doi:10.1029/2008GL036817.

Zhu, P., B. A. Albrecht, V. P. Ghate, and Z. D. Zhu (2010), Multiple scale simulations of stratocumulus clouds, *J. Geophys. Res.*, *115*, D23201, doi:10.1029/2010JD014400.

Ziervogel, K., L. McKay, B. Rhodes, C. L. Osburn, J. Dickson-Brown, C. Arnosti, and A. Teske (2012), Microbial activities and dissolved organic matter dynamics in oil-contaminated surface seawater from the Deepwater Horizon oil spill site, *PLoS ONE*, *7*, e34816, doi:10.1371/journal.pone.0034816.